J. Fluid Mech. (2015), *vol.* 769, *pp.* 26–45. © Cambridge University Press 2015
doi:10.1017/jfm.2015.94

Centrifugal instability in non-axisymmetric vortices

David Nagarathinam[1], A. Sameen[1] and Manikandan Mathur[1,†]

[1]Department of Aerospace Engineering, Indian Institute of Technology Madras, Chennai - 600036, India

(Received 8 April 2014; revised 27 January 2015; accepted 9 February 2015;
first published online 13 March 2015)

We study the centrifugal instability of non-axisymmetric vortices in the presence of an axial flow (w) and a background rotation (Ω_z) using the local stability approach. Analytically solving the local stability equations for an axisymmetric vortex with w and Ω_z, growth rates for wave vectors that are periodic upon evolution around a closed streamline are calculated. The resulting sufficient criterion for centrifugal instability in an axisymmetric vortex is then heuristically extended to non-axisymmetric vortices and written in terms of integral quantities and their derivatives with respect to the streamfunction on a streamline. The new criterion for non-axisymmetric vortices, which converges to the exact criterion of Bayly (*Phys. Fluids*, vol. 31, 1988, pp. 56–64) in the absence of background rotation and axial flow, is validated by comparisons with numerically calculated growth rates for two different anticyclonic vortices: the Stuart vortex (specified by the concentration parameter ρ, $0 < \rho \leqslant 1$) and the Taylor–Green vortex (specified by the aspect ratio E, $0 < E \leqslant 1$). With no axial velocity and finite background rotation, the criterion predicts a lower and an upper threshold of $|\Omega_z|$ between which centrifugal instability is present. We further demonstrate that the criterion represents an improvement over the criterion of Sipp & Jacquin (*Phys. Fluids*, vol. 12, 2000, pp. 1740–1748). Finally, in the presence of both axial velocity and background rotation, the criterion is shown to be accurate for large enough ρ and E.

Key words: vortex flows, vortex instability

1. Introduction

Vortical flows are ubiquitous in nature, often occurring in the form of large-scale structures like tornadoes, cyclones, vortex streets on the leeward side of islands and mountains; vortices are observed in several industrial shear flows too. Questions regarding the conditions under which a given vortex becomes unstable have therefore received considerable attention. In this paper, we derive an analytical criterion for centrifugal instability in an axisymmetric vortex with axial flow and background rotation, and then heuristically extend the criterion to non-axisymmetric vortices.

Early studies on the prediction of instability in an inviscid, axisymmetric vortex (with no axial flow and background rotation) subject to axisymmetric perturbations were carried out by Rayleigh (1917), who derived a necessary and sufficient condition

† Email address for correspondence: manims@ae.iitm.ac.in

for centrifugal instability based on physical arguments. Billant & Gallaire (2005) have extended Rayleigh's criterion to non-axisymmetric disturbances of any azimuthal wavenumber using large-axial-wavenumber asymptotics. For the more general scenario of a two-component, two-dimensional (2C2D), inviscid base flow, i.e. a base flow described by a velocity field $(u(x, y), v(x, y))$ in the Cartesian (x, y)-plane, with no background rotation, Bayly (1988) concluded that (i) the streamlines being convex closed curves in some region of the flow and (ii) the magnitude of the circulation decreasing outward are sufficient conditions for centrifugal instability.

Motivated by the velocity profiles in a trailing line vortex far downstream of a wing tip and in the region upstream of a vortex breakdown in experiments, Leibovich & Stewartson (1983) studied axisymmetric vortices with an axial flow (and no background rotation) to derive a centrifugal instability criterion using an asymptotic analysis for large-azimuthal-wavenumber perturbations. Billant & Gallaire (2013) have further extended the study of Leibovich & Stewartson (1983) to the case of large total wavenumber. Gallaire & Chomaz (2003*a*), using asymptotic expansions, have shown that centrifugal instability is active for all azimuthal wavenumbers in the axisymmetric screened Rankine vortex with a plug axial flow. Centrifugal instability has also been shown to be an important mechanism in the selection of the double-helix structure in realistic axisymmetric swirling jet flows (Gallaire & Chomaz 2003*b*). Recently, Mathur *et al.* (2014) investigated the effects of an axial flow on the centrifugal instability of Stuart vortices, a class of non-axisymmetric vortices that model mixing layer vortices. Solving the local stability equations numerically and also heuristically, deriving a criterion for centrifugal instability in non-axisymmetric vortices with no background rotation, Mathur *et al.* (2014) estimated a threshold value of the axial velocity gradient above which streamlines of the Stuart vortices become centrifugally unstable.

To model geophysical flows, Kloosterziel & van Heijst (1991) performed laboratory experiments and inferred, as a rule of thumb, that in a rotating fluid, only very weak anticyclonic, barotropic vortices are centrifugally stable, and only very strong cyclonic, barotropic vortices are centrifugally unstable. Three-dimensional direct numerical simulations (Potylitsin & Peltier 2003) have further shown the centrifugal destabilization of columnar anticyclonic vortices subjected to weak rotation. An analytical centrifugal instability criterion for axisymmetric vortices (with no axial flow) with background rotation was derived by Mutabazi, Normand & Wesfreid (1992). Three-dimensional linear stability analysis, using both the normal mode and the local stability approaches, of the non-axisymmetric Stuart vortices with background rotation have shown centrifugal instability to be a potential reason for instability in anticyclonic vortices (Leblanc & Cambon 1998; Potylitsin & Peltier 1999; Godeferd, Cambon & Leblanc 2001). In the Taylor–Green vortices of a specific aspect ratio with background rotation and no axial flow, Sipp, Lauga & Jacquin (1999) have shown the anticyclones to be centrifugally unstable if the Rossby number is larger than a threshold value. For the general case of any 2C2D flow in the presence of background rotation, Sipp & Jacquin (2000) used the local stability approach to derive a sufficient condition for centrifugal instability, which accurately captures most of the centrifugally unstable streamlines only in highly concentrated Stuart vortices.

To the best of our knowledge, no existing centrifugal instability criterion accounts for the combined effects of axial flow and background rotation. The current paper addresses this gap, and is organized as follows. Adopting the local stability approach (Lifschitz & Hameiri 1991), we derive an analytical centrifugal instability criterion for axisymmetric vortices, and then extend it to non-axisymmetric vortices in § 2.

The validity of our criterion in describing centrifugal instability in Stuart vortices and Taylor–Green vortices is investigated in § 3, followed by our discussion and conclusions in § 4.

2. Theory

We start by analytically solving the local stability equations for an inviscid, incompressible, steady, axisymmetric vortex (in the xy-plane) with an axial velocity, $w\boldsymbol{e}_z$, and a background rotation, $\boldsymbol{\Omega_B} = \Omega_z\boldsymbol{e}_z$, where $\boldsymbol{e}_z$ is the unit vector along the z direction. The base flow is described by a streamfunction $\psi(r)$, with the velocity components along $\boldsymbol{e_r}$, $\boldsymbol{e}_\theta$ and $\boldsymbol{e}_z$ in cylindrical polar coordinates given by $u_r = -(1/r)(\partial\psi/\partial\theta) = 0$, $u_\theta = \psi'$ and $u_z = w(r)$, respectively; the prime denotes the derivative with respect to $r = \sqrt{x^2 + y^2}$. The velocity field of the base flow is thus $\boldsymbol{U_B} = \psi'(r)\boldsymbol{e}_\theta + w(r)\boldsymbol{e}_z$.

2.1. *Local stability equations*

Linearized equations governing the velocity and pressure perturbations in an inviscid, incompressible flow are

$$\boldsymbol{\nabla}\cdot\boldsymbol{u} = 0, \tag{2.1}$$

$$\frac{\partial\boldsymbol{u}}{\partial t} + (\boldsymbol{U_B}\cdot\boldsymbol{\nabla})\boldsymbol{u} + (\boldsymbol{u}\cdot\boldsymbol{\nabla})\boldsymbol{U_B} + 2(\boldsymbol{\Omega_B}\times\boldsymbol{u}) + \boldsymbol{\nabla}P = 0, \tag{2.2}$$

where $\boldsymbol{u}$ and p are the perturbations in velocity and pressure, respectively, $P = p/\rho_0$ and ρ_0 is the constant density. We consider short-wavelength perturbations (Godeferd *et al.* 2001) in the limit of the WKBJ approximation:

$$(\boldsymbol{u}, p) = \exp\left(\mathrm{i}\frac{\phi(\boldsymbol{x}, t)}{\epsilon}\right)[(\boldsymbol{a}(\boldsymbol{x}, t), \pi(\boldsymbol{x}, t)) + \epsilon(\boldsymbol{a}_\epsilon(\boldsymbol{x}, t), \pi_\epsilon(\boldsymbol{x}, t)) + \cdots], \tag{2.3}$$

where ϕ is a real scalar function of position vector $\boldsymbol{x}$ and time t, ϵ a small parameter and $\boldsymbol{k} = \boldsymbol{\nabla}\phi$ the wave vector. Leading-order complex amplitudes of the velocity and pressure perturbations are $\boldsymbol{a}$ and π, respectively. Equations governing the evolution of $\boldsymbol{a}$ and $\boldsymbol{k}$ are given by Godeferd *et al.* (2001):

$$\frac{\mathrm{d}\boldsymbol{k}}{\mathrm{d}t} = [(\boldsymbol{\nabla}\times\boldsymbol{U_B})\times\boldsymbol{k} - (\boldsymbol{k}\cdot\boldsymbol{\nabla})\boldsymbol{U_B}], \tag{2.4}$$

$$\frac{\mathrm{d}\boldsymbol{a}}{\mathrm{d}t} = -\boldsymbol{\nabla}\boldsymbol{U_B}\cdot\boldsymbol{a} + \frac{2}{|\boldsymbol{k}|^2}[(\boldsymbol{\nabla}\boldsymbol{U_B}\cdot\boldsymbol{a})\cdot\boldsymbol{k}]\boldsymbol{k} - 2\boldsymbol{\Omega_B}\times\boldsymbol{a} + \frac{2}{|\boldsymbol{k}|^2}[(\boldsymbol{\Omega_B}\times\boldsymbol{a})\cdot\boldsymbol{k}]\boldsymbol{k}, \tag{2.5}$$

with $\pi = 0$ and $\boldsymbol{k}\cdot\boldsymbol{a} = 0$. The operator $\mathrm{d}/\mathrm{d}t = \partial/\partial t + \boldsymbol{U_B}\cdot\boldsymbol{\nabla}$ is the material time derivative in the base flow $\boldsymbol{U_B}$, i.e. derivative along fluid trajectories in the base flow.

2.2. *Growth rate for axisymmetric vortices*

We solve (2.5) for those wave vectors $\boldsymbol{k}$ that are periodic upon integrating equation (2.4) along one period of a three-dimensional streamline whose projection on the xy-plane is periodic. For a wave vector $\boldsymbol{k} = \alpha(t)\psi'\boldsymbol{e}_\theta + \beta(t)\psi'\boldsymbol{e}_r + \gamma\boldsymbol{e}_z$, where α and β evolve along the fluid trajectory in general, and $\mathrm{d}\gamma/\mathrm{d}t = 0$ for 3C2D base flows, the periodicity criterion for an axisymmetric base flow is (Mathur *et al.* 2014)

$$\alpha = \frac{-\gamma w'}{\psi'(\psi'' - \psi'/r)}, \tag{2.6}$$

which is invariant along a streamline. It was further shown by Mathur *et al.* (2014) that $\mathrm{d}\beta/\mathrm{d}t$ reduces to zero for an axisymmetric flow if (2.6) is satisfied. Therefore, α, β and γ are all invariant along a streamline for periodic wave vectors in an axisymmetric base flow. Since (2.4)–(2.5) are linear in $\boldsymbol{k}$, it suffices to consider unit periodic wave vectors, for which the procedure described in §4.1 in Mathur *et al.* (2014) allows us to write (2.5) as $[\mathrm{d}a_r/\mathrm{d}t\ \mathrm{d}a_\theta/\mathrm{d}t\ \mathrm{d}a_z/\mathrm{d}t] = \boldsymbol{C}[a_r\ a_\theta\ a_z]$, where $\boldsymbol{C}$ is a time-invariant 3×3 matrix. Eigenvalues of the coefficient matrix $\boldsymbol{C}$ are then the growth rates of the velocity perturbations. One of the three eigenvalues is zero, while the other two are given by

$$\sigma^2_{\boldsymbol{C}\{1,2\}} = (1-\beta^2\psi'^2)\left[\frac{4w'^2(r\Omega_z+\psi')^2}{(r\psi''-\psi')^2+r^2w'^2} - 2\left(\frac{\psi'}{r}+\Omega_z\right)\left(\psi''+\frac{\psi'}{r}+2\Omega_z\right)\right], \quad (2.7)$$

where the subscripts 1 and 2 correspond to the positive and negative roots of (2.7), respectively. We note that $\boldsymbol{k}$ being of unit magnitude imposes the constraint $\beta^2\psi'^2 \leqslant 1$.

2.3. *Instability criterion for axisymmetric vortices*

A streamline in an axisymmetric vortex is unstable if the eigenvalues in (2.7) satisfy $\sigma^2_{\boldsymbol{C}\{1,2\}} > 0$. Since $0 \leqslant \beta^2\psi'^2 \leqslant 1$, the criterion for instability reduces to

$$(\sigma^*_{\boldsymbol{C}\{1,2\}})^2 = \left[\frac{4w'^2(r\Omega_z+\psi')^2}{(r\psi''-\psi')^2+r^2w'^2} - 2\left(\frac{\psi'}{r}+\Omega_z\right)\left(\psi''+\frac{\psi'}{r}+2\Omega_z\right)\right] > 0, \quad (2.8)$$

where $\sigma^*_{\boldsymbol{C}\{1,2\}}$ are the values of $\sigma_{\boldsymbol{C}\{1,2\}}$ evaluated at $\beta = 0$. For unstable streamlines, $\sigma^*_{\boldsymbol{C}\{1\}}$ represents the maximum growth rate, with the corresponding most unstable wave vector given by $\beta = 0$. It is noteworthy that $\beta = 0$ corresponds to the periodic wave vector with the smallest angle $\theta = \theta_{min}$ made with the z-axis (Mathur *et al.* 2014). In the rest of this paper, we replace $\sigma^*_{\boldsymbol{C}\{1\}}$ by $\sigma^*_{\boldsymbol{C}}$. The criterion in (2.8) can also be obtained by replacing ψ by $\psi + \Omega_z r^2/2$ in the centrifugal instability criterion for axisymmetric vortices with an axial velocity and no background rotation (Leibovich & Stewartson 1983; Eckhoff 1984; Mathur *et al.* 2014).

In the absence of axial flow and background rotation, i.e. $\mathrm{d}w/\mathrm{d}\psi = 0$ and $\Omega_z = 0$, the criterion (2.8) reduces to the criterion for centrifugal instability of an axisymmetric flow subjected to axisymmetric perturbations: $(\psi'/r)(\psi'' + \psi'/r) < 0$, derived by Rayleigh (1917) based on the displaced-particle argument in a system whose angular momentum is conserved. Without background rotation ($\Omega_z = 0$), the criterion (2.8) reduces to the centrifugal instability criterion derived using the normal mode approach (Leibovich & Stewartson 1983) and the local stability approach (Mathur *et al.* 2014). In the absence of axial flow ($\mathrm{d}w/\mathrm{d}\psi = 0$), the criterion (2.8) reduces to the criterion for centrifugal instability of an axisymmetric vortex with a background rotation: $(\psi'/r + \Omega_z)(\psi'' + \psi'/r + 2\Omega_z) < 0$, derived using both the displaced-particle argument (Mutabazi *et al.* 1992) and the local stability approach (Sipp & Jacquin 2000).

2.4. *Extension to non-axisymmetric vortices*

Based on the heuristic approach of Mathur *et al.* (2014), we now extend the analytical criterion (2.8) to the case of a non-axisymmetric vortex and numerically evaluate its validity for the specific cases of Stuart vortices and Taylor–Green vortices. Replacing

$\mathrm{d}/\mathrm{d}r$ by $\psi'\mathrm{d}/\mathrm{d}\psi$ in (2.8), we get

$$(\sigma^*_{\boldsymbol{C}\{1,2\}})^2 = \left[\frac{4(\mathrm{d}w/\mathrm{d}\psi)^2(\Omega_z+\psi'/r)^2}{r^2(\mathrm{d}(\psi'/r)/\mathrm{d}\psi)^2+(\mathrm{d}w/\mathrm{d}\psi)^2} - 2\left(\frac{\psi'}{r}+\Omega_z\right)\left(\frac{\psi'}{r}\frac{\mathrm{d}(r\psi')}{\mathrm{d}\psi}+2\Omega_z\right)\right] > 0. \tag{2.9}$$

We now choose to write the criterion in (2.9) in terms of $\Gamma = 2\pi r\psi'$ and $T = 2\pi r/\psi'$, where the integral quantities Γ and T are the circulation and the time period of the streamline, respectively. Specifically, replacing ψ' by $(\Gamma/T)^{1/2}$ and r by $(\Gamma T)^{1/2}/2\pi$, the criterion (2.9) reduces to

$$(\sigma^*_{\boldsymbol{C}\{1,2\}})^2 = \frac{4(\mathrm{d}w/\mathrm{d}\psi)^2(\Omega_z+2\pi/T)^2}{(\Gamma/T^3)(\mathrm{d}T/\mathrm{d}\psi)^2+(\mathrm{d}w/\mathrm{d}\psi)^2} - 2\left(\frac{2\pi}{T}+\Omega_z\right)\left(\frac{1}{T}\frac{\mathrm{d}\Gamma}{\mathrm{d}\psi}+2\Omega_z\right) > 0, \tag{2.10}$$

an expression that can be evaluated for any non-axisymmetric vortex. The base flow quantities that appear in criterion (2.10) are dependent only on ψ, i.e. every streamline (specified by a unique value of ψ) has a corresponding unique value of T, Γ, $\mathrm{d}T/\mathrm{d}\psi$, $\mathrm{d}\Gamma/\mathrm{d}\psi$ and $\mathrm{d}w/\mathrm{d}\psi$, rendering the criterion easy to evaluate in comparison to criteria that require the velocity field at every point on the streamline. To the best of our knowledge, criterion (2.10) represents the first effort to derive a criterion for centrifugal instability in non-axisymmetric vortices with an axial flow and a background rotation.

The heuristic approach to express criterion (2.8) in terms of Γ and T is motivated by their significant roles in the centrifugal instability of non-axisymmetric vortices without axial flow and background rotation (Bayly 1988) and the periodicity condition for wave vectors (Mathur *et al.* 2014), respectively. While the criterion in (2.10) remains exactly valid for axisymmetric vortices, its validity for non-axisymmetric vortices is to be investigated. Furthermore, though the expression of (2.8) in terms of Γ, T and their derivatives with respect to ψ is not uniquely defined, our choice ensures that the criterion in (2.10) converges to the exact criterion of Bayly (1988) in the limit of $\mathrm{d}w/\mathrm{d}\psi = 0$ and $\Omega_z = 0$. Finally, the coupling between $\mathrm{d}w/\mathrm{d}\psi$ and Ω_z in criterion (2.10) means one cannot look at their effects in isolation to derive a criterion for a flow with non-zero $\mathrm{d}w/\mathrm{d}\psi$ and Ω_z.

3. Results

In this paper, we investigate the validity of criterion (2.10) in describing the centrifugal instability in two specific vortex models: (i) Stuart vortices (Stuart 1967) and (ii) steady, flattened Taylor–Green vortices (Taylor & Green 1937), in the presence of axial flow and background rotation. The validations are carried out via comparisons with the numerical solutions of (2.4)–(2.5).

The streamfunction describing Stuart vortices centred at the origin in the xy-plane is given by Godeferd *et al.* (2001)

$$\psi(x, y) = \log(\cosh y - \rho\cos x), \tag{3.1}$$

where ρ $(0 < \rho \leqslant 1)$ is the concentration parameter. As ρ decreases from 1 to smaller values, the vorticity distribution goes from highly concentrated around the origin to more widely spread away from the origin. Streamlines for four different values of ρ are plotted in figure 5 of Godeferd *et al.* (2001). Defining $\tilde{\psi} = (\psi - \psi_{min})/(\psi_{max} - \psi_{min})$, where $\psi_{max} = \log(1+\rho)$ and $\psi_{min} = \log(1-\rho)$, we

consider only those streamlines that lie in the range $0 < \tilde{\psi} < 1$, thus restricting our studies to closed streamlines. We note, however, that the open streamlines in Stuart vortices may be susceptible to centrifugal instability too.

An isolated, steady, flattened Taylor–Green vortex with anticlockwise fluid motion, centred at the origin is described by the following streamfunction (Sipp & Jacquin 1998; Sipp *et al.* 1999):

$$\psi(x, y) = \sin(x - \pi/2)\sin(Ey + \pi/2), \tag{3.2}$$

where E $(0 < E \leqslant 1)$ is the aspect ratio of the vortex. Denoting the x-coordinate of the intersection between a streamline and the positive x-axis by x_0, we consider only those streamlines that lie inside the vortex centred at the origin, i.e. $0 < x_0 < \pi/2$. This anticlockwise vortex corresponds to the upper right quadrant of figure 1 in Sipp *et al.* (1999).

As discussed in § 2.4, the criterion in (2.10) is exact for axisymmetric vortices whereas the extent of its validity to describe centrifugal instability in non-axisymmetric vortices has to be numerically established. We therefore start by quantifying the extent of non-axisymmetry of the streamlines in the two vortex models we consider in this paper. Specifically, we define the extent of non-axisymmetry for any streamline as (Mathur *et al.* 2014)

$$S = \frac{r_\sigma(x_0)}{\bar{r}(x_0)}, \tag{3.3}$$

where r_σ and $\bar{r}$ are the standard deviation and mean, respectively of $r(i) = \sqrt{x(i)^2 + y(i)^2}$, with $(x(i), y(i))$ being the ith point on the streamline which intersects the positive x-axis at $(x_0, 0)$. For the calculation of S, we represent every streamline by 1000 points that are equispaced in terms of the distance measured along the streamline. The smaller the value of S, the closer the streamline is to a circular shape.

Figures 1(*a*) and 1(*b*) show the contour lines of S as a function of the streamline and the corresponding vortex model parameter for Stuart vortices and Taylor–Green vortices, respectively. In the Stuart vortices (figure 1*a*), for a fixed $\tilde{\psi}$, S is larger for smaller ρ, implying that streamlines become more strongly non-axisymmetric as ρ decreases. For a fixed value of ρ, S increases with $\tilde{\psi}$, i.e. streamlines away from the origin are more strongly non-axisymmetric than the ones close to the origin. At $\rho = 1$, S increases from 0 for the innermost streamlines to around 0.177 for streamlines at the edge of the vortex.

In the Taylor–Green vortices (figure 1*b*), streamlines become more non-axisymmetric when the aspect ratio E moves away from unity. For a fixed x_0, as seen in figure 1(*b*), S is smaller for larger E. For a fixed small enough value of E $(0 < E \lesssim 0.5)$, all the streamlines correspond to almost the same value of S, whereas for larger E, there is a sudden increase in S as we approach the outer edge of the vortex. At $E = 1$, S increases from 0 for the innermost streamlines to around 0.092 for streamlines at the edge of the vortex.

To evaluate the validity of criterion (2.10), we also compute the actual growth rate σ_N by numerically solving (2.4)–(2.5) for periodic wave vectors with $\theta = \theta_{min}$. As shown in § 2.3, since the most unstable wave vector for centrifugal instability corresponds to $\beta = 0$, it suffices to consider only the wave vector with $\beta = 0$, i.e. $\theta = \theta_{min}$. To compute σ_N we use the numerical algorithm described in Mathur *et al.* (2014). Owing to the presence of very small numerical errors that result from the

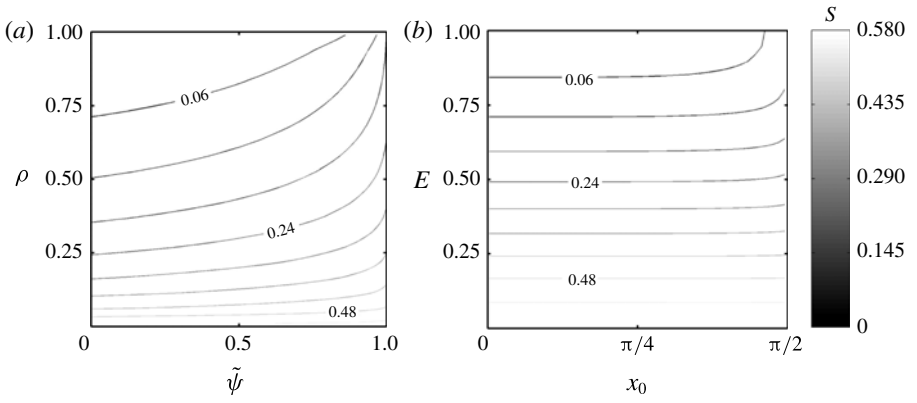

FIGURE 1. The non-axisymmetry parameter S, defined in (3.3), as a function of the streamline and the vortex model parameter for (*a*) Stuart vortices and (*b*) Taylor–Green vortices. Both plots show the contour lines corresponding to the same set of nine different values of S equispaced between 0.06 and 0.54.

machine accuracy and the numerical schemes used, which in turn would wrongly pick up stable regimes as unstable, we assign any value of $\mathrm{Re}[\sigma_N]$ smaller than 10^{-14} to zero. Here, Re denotes the real part.

On a given streamline inside a two-dimensional vortex centred at the origin, the influence of the axial flow on its stability is completely described by the parameter τ (Mathur *et al.* 2014):

$$\tau = \frac{(\mathrm{d}w/\mathrm{d}\psi)v(x_0, 0)}{\omega}, \tag{3.4}$$

where the streamline intersects the positive x-axis at $(x_0, 0)$ and $\omega = \nabla^2\psi$ is the constant vorticity along $\boldsymbol{e}_z$ associated with the streamline. We now proceed to investigate various regimes in the parameter space of ρ (or E depending on the vortex model), Ω_z and τ, concluding with the combined effects of axial flow and background rotation on the centrifugal instability in Stuart vortices and Taylor–Green vortices. Our validation studies in this paper are restricted to anticyclonic vortices, i.e. $\Omega_z < 0$, which previous studies have shown to be more susceptible to instability than cyclonic vortices when there is no axial flow (Hopfinger & van Heijst 1993). Furthermore, Sipp *et al.* (1999) have shown that centrifugal instability in Taylor–Green vortices with no axial flow is activated by anticyclonic rotation but not cyclonic rotation.

3.1. *No axial flow* ($\mathrm{d}w/\mathrm{d}\psi = 0$)*, no background rotation* ($\Omega_z = 0$)

The centrifugal instability criterion in (2.10) reduces to $\mathrm{d}\Gamma/\mathrm{d}\psi < 0$ for flows with no axial velocity and background rotation, i.e. 2C2D flows with $\Omega_z = 0$. Based on this limiting criterion, which is consistent with the results of Bayly (1988), the Stuart vortices and the Taylor–Green vortices are both centrifugally stable for $\mathrm{d}w/\mathrm{d}\psi = 0$ and $\Omega_z = 0$, i.e. the two base flows described by (3.1) and (3.2) satisfy $\mathrm{d}\Gamma/\mathrm{d}\psi > 0$ for all the streamlines inside the respective vortices.

3.2. *Axial flow with no background rotation*

In the limit of $\Omega_z = 0$, the analytical criterion (2.10) reduces to the criterion of Mathur *et al.* (2014) for centrifugal instability in non-axisymmetric vortices with an axial flow

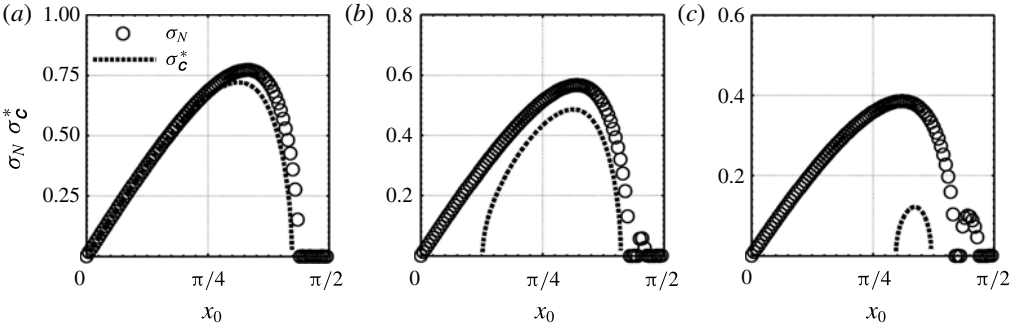

FIGURE 2. A plot of $\mathrm{Re}[\sigma_N]$, σ_c^* as a function of x_0 for Taylor–Green vortices with (*a*) $E = 1$ and $\Omega_z = 0$, (*b*) $E = 0.75$ and $\Omega_z = 0$ and (*c*) $E = 0.5$ and $\Omega_z = 0$. Values of $\mathrm{Re}[\sigma_c^*] \leqslant 0$ are not shown. All the plots correspond to $\tau = 2$.

and no background rotation. Mathur *et al.* (2014) have shown that there is always a threshold value of τ above which a given streamline in the Stuart vortices becomes centrifugally unstable; their criterion accurately predicts the threshold value of τ even for small values of ρ, for which the base flow is strongly non-axisymmetric.

An interesting result from Mathur *et al.* (2014) is that, in the limit of a strong axial flow with no background rotation, the criterion in (2.10) seems to be quantitatively accurate in describing centrifugal instability in Stuart vortices for all the streamlines with $S \lesssim 0.2$. To test the robustness of this conclusion of Mathur *et al.* (2014), we perform a quantitative comparison between σ_N and σ_c^* for Taylor–Green vortices with no background rotation and a strong axial flow.

Figure 2 shows the variations of σ_N and σ_c^* as a function of x_0 for $E = 1, 0.75$ and 0.5 with $\Omega_z = 0$ and $\tau = 2$. We see that σ_c^* is in close agreement with σ_N for $E = 1$ (figure 2*a*), for which the extent of non-axisymmetry S increases from 0 to 0.09 as x_0 increases from 0 to $\pi/2$. The agreement between σ_c^* and σ_N is reasonably good for $E = 0.75$ (figure 2*b*) too, a scenario where S varies from 0.1 to 0.135 across the streamlines in the vortex. For $E = 0.5$ (figure 2*c*), however, the prediction based on σ_c^* is poor and is attributed to $S \geqslant 0.23$ for all the streamlines (as seen in figure 1*b*). In summary, the criterion of $S \lesssim 0.2$ for σ_c^* to accurately describe centrifugal instability with no background rotation and large axial flow is reasonably valid for Taylor–Green vortices too. Furthermore, since the Taylor–Green vortices are centrifugally stable at $\Omega_z = 0$ and $\tau = 0$, finite growth rates for all three values of E at $\Omega_z = 0$ and $\tau = 2$ show that centrifugal instability emerges beyond a threshold magnitude of axial flow.

3.3. *Background rotation with no axial flow*

We now consider the effect of background rotation in the absence of axial flow. Substituting $\mathrm{d}w/\mathrm{d}\psi = 0$ reduces criterion (2.10) to

$$-(\sigma_{c\{1,2\}}^*)^2 = 2\left(\frac{2\pi}{T} + \Omega_z\right)\left(\frac{1}{T}\frac{\mathrm{d}\Gamma}{\mathrm{d}\psi} + 2\Omega_z\right) < 0. \tag{3.5}$$

Sipp & Jacquin (2000) have previously proposed an alternative criterion for instability of two-dimensional flows (without an axial velocity) subject to background rotation. Their sufficient criterion for instability on a streamline with streamfunction ψ is

$$-\sigma_{S\&J}^2(\psi) = \Delta_{S\&J}(\psi) = \max\left[2\left(\frac{V}{R} + \Omega_z\right)\left(W + 2\Omega_z\right)\right] < 0, \tag{3.6}$$

V being the local norm of the velocity, R the local radius of curvature on the streamline and W the vorticity associated with the streamline. The criterion (3.6), referred to as S&J's criterion in the rest of this paper, is not very accurate for highly non-axisymmetric Stuart vortices (Sipp & Jacquin 2000).

3.3.1. *Stuart vortices*

Using the criterion in (2.10), we classify the base flow with a specific set of values for (ρ, Ω_z) as unstable if there exists at least one streamline in the range $0 < \tilde{\psi} < 1$ for which $\mathrm{Re}[\sigma^*_{\boldsymbol{C}}] > 0$. The identification of instability based on S&J's criterion in (3.6) and the numerical solution use $\sigma_{S\&J}$ and σ_N, respectively. The calculation of $\sigma^*_{\boldsymbol{C}}$, $\sigma_{S\&J}$ and σ_N is performed for $0.01 \leqslant x_0 \leqslant 3$, thus skipping the streamlines in the range $3 < x_0 \leqslant \pi$. We note here that $\mathrm{Re}[\sigma_N]$ may sometimes be greater than zero due to the presence of non-centrifugal (elliptic, hyperbolic) instabilities.

Plotted in figure 3 are the curves that delineate the stable and unstable regions based on the $\mathrm{Re}[\sigma^*_{\boldsymbol{C}}] > 0$ (solid line) and $\mathrm{Re}[\sigma_{S\&J}] > 0$ (dashed line) criteria. The background grey colour corresponds to regions with $\mathrm{Re}[\sigma_N] > 0$. Both our criterion (3.5) and S&J's criterion (3.6) predict that the flow is centrifugally stable at $\Omega_z = 0$ for every ρ. Owing to the presence of elliptic and/or hyperbolic instabilities that occur for $\Omega_z = 0$ (Godeferd *et al.* 2001), $\mathrm{Re}[\sigma_N]$ is greater than zero and hence the background colour at and around $\Omega_z = 0$ is grey. Based on criterion (3.5), for all ρ, as the magnitude of background rotation increases from $\Omega_z = 0$, there exists a threshold value $|\Omega_z|_{1,\boldsymbol{C}}$ (which is a function of ρ) above which the flow becomes centrifugally unstable (the $\boldsymbol{C}$ in the subscript refers to predictions based on $\sigma^*_{\boldsymbol{C}}$ in criterion (3.5)). For $0.5 \lesssim \rho < 1$, there is a good agreement in this threshold value of $|\Omega_z|$ between criterion (3.5) and S&J's criterion. For smaller values of ρ, i.e. $\rho < 0.43$, corresponding to strongly non-axisymmetric vortices, S&J's criterion predicts the flow to be stable for all values of Ω_z whereas our criterion continues to predict a threshold value of $|\Omega_z|$ above which the flow becomes centrifugally unstable.

For $\rho \leqslant 0.67$, as we increase the $|\Omega_z|$ beyond the first threshold $|\Omega_z|_{1,\boldsymbol{C}}$, the numerical growth rate σ_N predicts that there is a threshold $|\Omega_z|_{2,N}$ (which is a function of ρ) above which the flow becomes stable (the N in the subscript refers to predictions based on the numerical growth rate σ_N). This is indicated by the background colour changing from grey to white beyond $|\Omega_z|_{2,N}$ for $\rho \leqslant 0.67$. The corresponding threshold $|\Omega_z|_{2,\boldsymbol{C}}$ based on $\sigma^*_{\boldsymbol{C}}$ is in remarkable agreement with the numerics for the prediction of $|\Omega_z|_{2,N}$. S&J's criterion, however, underpredicts $|\Omega_z|_{2,N}$ for $0.43 \leqslant \rho < 0.74$ and fails to predict any instability for $\rho < 0.43$. In summary, the criterion based on $\sigma^*_{\boldsymbol{C}}$ is very accurate in identifying the centrifugally unstable domain in the ρ–Ω_z plane. We now proceed to evaluate the validity of the $\sigma^*_{\boldsymbol{C}}$ criterion for individual trajectories.

In figure 4, we plot σ_N, $\sigma^*_{\boldsymbol{C}}$ and $\sigma_{S\&J}$ as a function of $\tilde{\psi}$ for three different pairs of (ρ, Ω_z), indicated by the three points marked by a star in figure 3. For $\rho = 0.77$, $\Omega_z = -2.318$, shown in figure 4(*a*), there is almost an exact agreement between the numerics (circles) and the $\sigma^*_{\boldsymbol{C}}$ criterion (dashed line) for the range of centrifugally unstable streamlines ($0.12 \leqslant \tilde{\psi} \leqslant 0.24$) and the corresponding growth rates. The S&J criterion (solid line) identifies only a part of the unstable streamlines ($0.12 \leqslant \tilde{\psi} \leqslant 0.18$), with the maximum growth rate underpredicted by 54 %. For $\rho = 0.57$, $\Omega_z = -0.894$, the case presented in figure 4(*b*), $\sigma^*_{\boldsymbol{C}}$ identifies the range $0.27 \leqslant \tilde{\psi} \leqslant 0.48$ as centrifugally unstable while the corresponding range based on σ_N and $\sigma_{S\&J}$ are $0.27 \leqslant \tilde{\psi} \leqslant 0.53$ and $0.27 \leqslant \tilde{\psi} \leqslant 0.3$, respectively. Here $\sigma^*_{\boldsymbol{C}}$ underpredicts

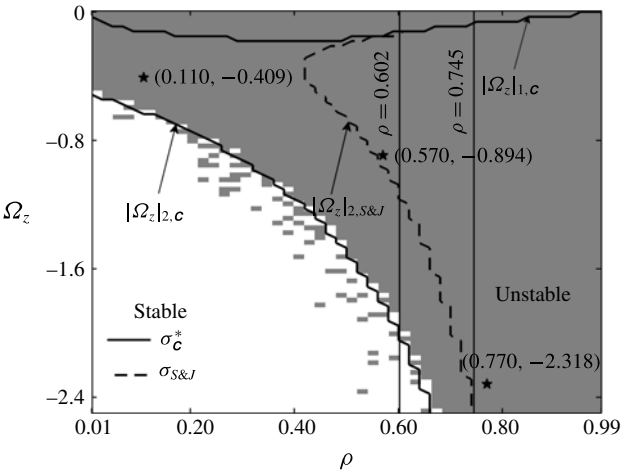

FIGURE 3. Contours delineating the stable and unstable flow regimes of Stuart vortices without an axial flow ($\tau = 0$). The solid and dashed lines are obtained based on σ_c^* (criterion (3.5)) and $\sigma_{S\&J}$ (criterion (3.6)), respectively. The background grey colour indicates regions with $\mathrm{Re}[\sigma_N] > 0$ obtained numerically. Stars indicate the specific cases shown in figure 4. Vertical lines at $\rho = 0.602$ and 0.745 correspond to the cases presented in figure 5.

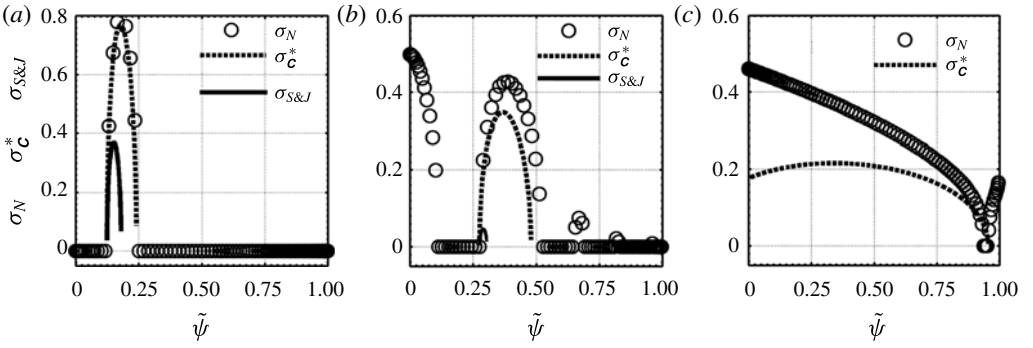

FIGURE 4. A plot of $\mathrm{Re}[\sigma_N]$, σ_c^*, $\sigma_{S\&J}$ as a function of $\tilde{\psi}$ for Stuart vortices with (*a*) $(\rho, \Omega_z) = (0.77, -2.318)$, (*b*) $(\rho, \Omega_z) = (0.57, -0.894)$ and (*c*) $(\rho, \Omega_z) = (0.11, -0.409)$. The three cases correspond to the stars on the ρ–Ω_z plane in figure 3. Values of $\mathrm{Re}[\sigma_c^*, \sigma_{S\&J}] \leqslant 0$ are not shown. All the plots correspond to $\tau = 0$.

the maximum growth rate by only 18.6 % whereas $\sigma_{S\&J}$ is an order of magnitude smaller than σ_N. Finally, for $\rho = 0.11$, $\Omega_z = -0.409$, the strongly elliptic scenario presented in figure 4(*c*), σ_c^* correctly predicts the centrifugally unstable streamlines in the range $0 \lesssim \tilde{\psi} \lesssim 0.95$ but with the growth rates around half of σ_N for the streamlines close to the origin; $\sigma_{S\&J}$ does not predict any streamline in the range $0 < \tilde{\psi} < 1$ to be unstable.

To evaluate the validity of our criterion and S&J's criterion over the entire range of Ω_z for a given ρ, we plot a colourmap of σ_N, σ_c^* and $\sigma_{S\&J}$ as a function of $\tilde{\psi}$ and Ω_z for $\rho = 0.745$ and $\rho = 0.602$ in figure 5. For both $\rho = 0.745$ and $\rho = 0.602$,

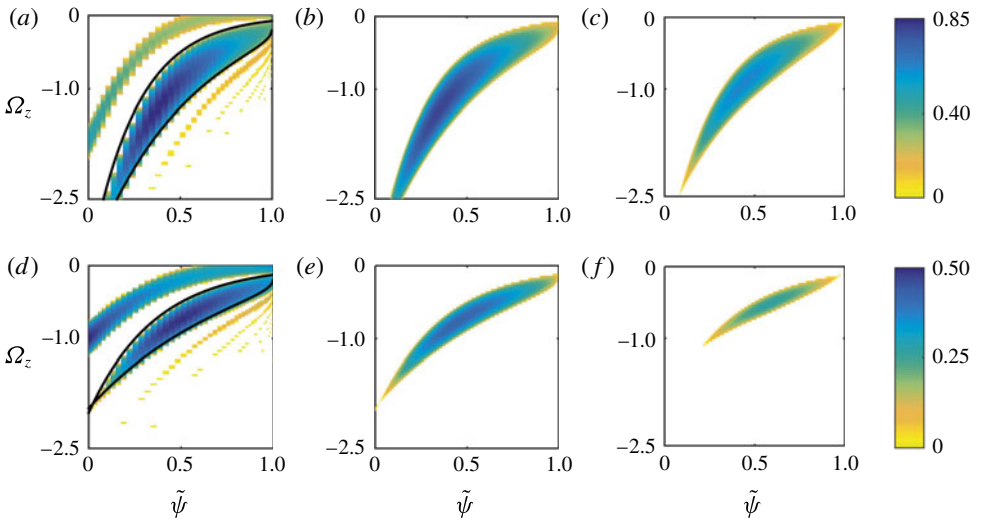

FIGURE 5. (Colour online) (*a*,*d*) σ_N, (*b*,*e*) σ_C^* and (*c*,*f*) $\sigma_{S\&J}$ plotted as a function of $\tilde{\psi}$ and Ω_z for Stuart vortices with (*a–c*) $\rho = 0.745$ and (*d–f*) $\rho = 0.602$. White regions in the plots correspond to $\mathrm{Re}[\sigma_N, \sigma_C^*, \sigma_{S\&J}] \leqslant 0$. All the plots correspond to $\tau = 0$. The two solid black curves in each of (*a*) and (*d*), described by (4.2) and (4.3), correspond to the boundaries of the unstable domain in (*b*) and (*e*), respectively.

σ_N displays two dominant sub-domains of instability, with the sub-domain occurring for smaller $|\Omega_z|$ likely to be a non-centrifugal-type instability, as was discussed to explain the grey background around $\Omega_z = 0$ in figure 3. The sub-domain of instability, captured by σ_N, occurring for larger $|\Omega_z|$ is quantitatively similar to the sub-domain of centrifugal instability identified by σ_C^*. For $\rho = 0.745$, $\sigma_{S\&J}$ identifies a relatively smaller sub-domain of instability with the maximum growth rate being 26.6 % smaller than σ_N. For $\rho = 0.602$, $\sigma_{S\&J}$ fails to identify a significant portion of the centrifugally unstable sub-domain, while σ_C^* continues to be accurate in capturing the range of unstable streamlines.

In the centrifugal instability sub-domains of instability identified in the σ_N plots in figure 5(*a*,*d*), each streamline corresponds to a lower threshold $|\Omega_z|_{L,N}$ and an upper threshold $|\Omega_z|_{U,N}$ between which it is centrifugally unstable. The corresponding thresholds based on σ_C^*, referred to as $|\Omega_z|_{L,C}$ and $|\Omega_z|_{U,C}$, are indicated by the black curves in figure 5(*a*,*d*). We observe that σ_C^* predicts the centrifugally unstable domain on the $\tilde{\psi}$–Ω_z plane accurately for both $\rho = 0.745$ and $\rho = 0.602$.

For smaller values of ρ (the results of which are not shown in the figures), corresponding to strongly non-axisymmetric vortices, the sub-domain of centrifugal instability in the $\tilde{\psi}$–Ω_z plane is observed to be smaller than that for larger ρ. The criterion based on σ_C^* is reasonably accurate even for $\rho = 0.235$, whereas $\sigma_{S\&J}$ fails to predict any unstable streamlines for $\rho \leqslant 0.43$.

3.3.2. *Taylor–Green vortices*

Similar to the analysis in § 3.3.1, a given (E, Ω_z) pair is termed unstable based on three different criteria, i.e. the sign of $\mathrm{Re}[\sigma_N]$, $\mathrm{Re}[\sigma_C^*]$ or $\mathrm{Re}[\sigma_{S\&J}]$ being positive for at least one streamline in the range $0 < x_0 < \pi/2$. The calculation of σ_C^*, $\sigma_{S\&J}$ and σ_N is performed for $0.01 \leqslant x_0 \leqslant 1.55$, thus skipping the streamlines in the range

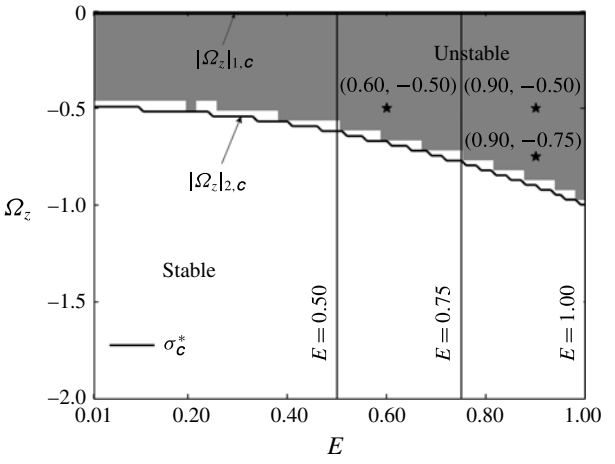

FIGURE 6. Contours delineating the stable and unstable flow regimes of Taylor–Green vortices without an axial flow ($\tau = 0$). The domain bound within the solid lines marked as $|\Omega_z|_{1,c}$ and $|\Omega_z|_{2,c}$ is the unstable (E, Ω_z) parameter space based on σ_c^*. The background grey color indicates unstable regions with $\mathrm{Re}[\sigma_N] > 0$. Note that $\sigma_{S\&J}$ (criterion (3.6)) does not predict instability over the entire E–Ω_z plane considered. Stars indicate the specific cases shown in figure 7. Vertical lines at $E = 0.5$, $E = 0.75$ and $E = 1$ correspond to the cases presented in figure 8.

$1.55 < x_0 \leqslant \pi/2$. The unstable domain, in the two-dimensional parameter space of (E, Ω_z), evaluated based on σ_c^* is bound within the solid lines marked as $|\Omega_z|_{1,c}$ and $|\Omega_z|_{2,c}$ in figure 6. The corresponding unstable domain based on σ_N is shown with a grey background. The criterion based on $\sigma_{S\&J}$ predicts every streamline to be stable over the entire (E, Ω_z) domain considered in figure 6.

For $\Omega_z = 0$, the Taylor–Green vortices are centrifugally stable owing to the positive sign of $\mathrm{d}\Gamma/\mathrm{d}\psi$; σ_N, however, suggests that the vortex is susceptible to a non-centrifugal-type instability, as indicated by the grey background at $\Omega_z = 0$ in figure 6. For each value of E, σ_c^* predicts a small threshold of $|\Omega_z| = |\Omega_z|_{1,c}$ (of the order of 0.01) above which the vortex becomes centrifugally unstable. $|\Omega_z|_{1,c}$, as to be discussed in § 4, would be zero if the outermost streamline corresponding to $x_0 = \pi/2$ is included in the calculations. Upon increasing $|\Omega_z|$ further, σ_c^* identifies another threshold $|\Omega_z| = |\Omega_z|_{2,c}$, above which the Taylor–Green vortex becomes centrifugally stable. The functional dependence of $|\Omega_z|_{2,c}$ on E is in reasonably good quantitative agreement with the predictions based on σ_N, i.e. the lower solid curve captures the lower boundary of the grey domain in figure 6 reasonably well.

We now define the Rossby number for a fixed E and Ω_z as (Sipp *et al.* 1999)

$$Ro = \frac{\omega_{max}}{2|\Omega_z|}, \tag{3.7}$$

where ω_{max} is the maximum vorticity among all the streamlines in the range $0 < x_0 < \pi/2$. One can now write $|\Omega_z|_{2,c}$ as an equivalent Rossby number below which the vortex is centrifugally stable at a given E. For $E = 0.5$, we find that σ_c^* predicts the flow to be centrifugally stable for $Ro < 1.003$. This result is in close agreement with the result of Sipp *et al.* (1999) that for Taylor–Green cells with an aspect ratio $E = 2$, anticyclones undergo centrifugal instability if the Rossby number satisfies $Ro > 1$.

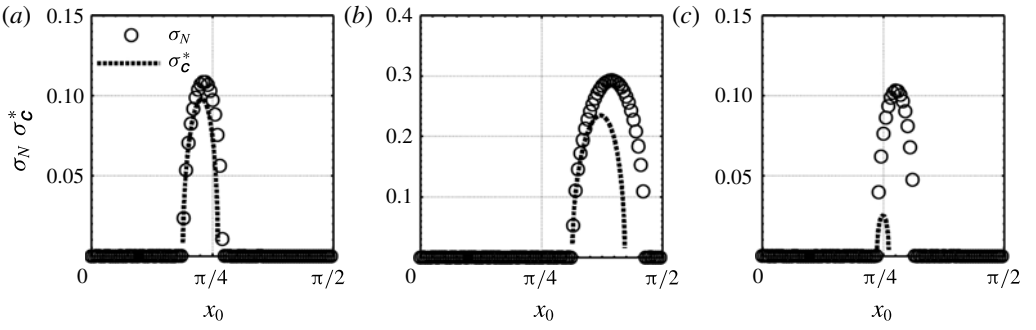

FIGURE 7. A plot of Re[σ_N] and σ_C^* as a function of x_0 for Taylor–Green vortices with (*a*) $(E, \Omega_z) = (0.9, -0.75)$, (*b*) $(E, \Omega_z) = (0.9, -0.5)$ and (*c*) $(E, \Omega_z) = (0.6, -0.5)$. The three cases correspond to the stars on the E–Ω_z plane in figure 6. Values of Re[σ_C^*] $\leqslant 0$ are not shown. All the plots correspond to $\tau = 0$.

We note here that $E = 0.5$ and $E = 2$ correspond to equivalent vortices that share the same shape for all the streamlines. Writing $|\Omega_z|_{2,C}$ as an equivalent Rossby number for all values of E, we further find that Ro at the lower solid black curve in figure 6 is in the range 1–1.005, thus leading to the conclusion that the criterion $Ro < 1$ for centrifugal stability in Taylor–Green vortices is valid for all values of E when there is no axial flow. Performing a similar calculation for Stuart vortices with $\tau = 0$, we find that $|\Omega_z|_{2,C}$ shown in figure 3 corresponds to $Ro \approx 1$ too for all values of ρ.

In figure 7, we plot σ_C^* and σ_N as a function of x_0 for three different pairs of values of (E, Ω_z), corresponding to the three stars in figure 6. For $E = 0.9$, $\Omega_z = -0.75$ (figure 7*a*), σ_N identifies unstable streamlines to be in the range $0.6 < x_0 < 0.85$, with a maximum growth rate of 0.109. Correspondingly, σ_C^* predicts the centrifugally unstable streamlines to be in the range $0.59 < x_0 < 0.82$, with 0.098 as the maximum growth rate. For $E = 0.9$, $\Omega_z = -0.5$, σ_C^* underpredicts the maximum growth rate by around 20 %, whereas the range of unstable streamlines is captured somewhat accurately (figure 7*b*). In figure 7(*c*), which corresponds to $E = 0.6$, $\Omega_z = -0.5$, σ_C^* further underpredicts both the maximum growth rate and the range of unstable streamlines. In summary, while the criterion based on σ_C^* accurately captures the overall unstable domain in the E–Ω_z plane, the predictions on the range of unstable streamlines and the corresponding growth rates deviate from those based on σ_N for some individual pairs of (E, Ω_z). We now proceed to investigate the accuracy of σ_C^* over a finite range of Ω_z.

Colourmaps of the growth rate as a function of x_0 and Ω_z for Taylor–Green vortices with $E = 1$, 0.75 and 0.5 and $\tau = 0$ are shown in figure 8. For $E = 1$, as shown by the σ_N distribution in figure 8(*a*), an instability emerges near the outermost streamline ($x_0 = \pi/2$) as $|\Omega_z|$ is increased from zero. The instability moves towards smaller values of x_0 as $|\Omega_z|$ increases before disappearing below a threshold of around $\Omega_z = -1$. Similar to the case of Stuart vortices, at each x_0 in figure 8(*a*), there exists a lower and an upper threshold $|\Omega_z| = |\Omega_z|_{L,N}$ and $|\Omega_z| = |\Omega_z|_{U,N}$ between which the corresponding streamline is centrifugally unstable; $|\Omega_z|_{L,N}$ decreases as x_0 increases whereas $|\Omega_z|_{U,N} - |\Omega_z|_{L,N}$ is larger for the outer streamlines close to $x_0 = \pi/2$ in comparison to those close to $x_0 = 0$. For each E, the maximum $|\Omega_z|_{U,N}$ among all the streamlines is equal to the $|\Omega_z|_{2,N}$ defined earlier in the discussion of figure 6. The σ_C^* distribution, shown in figure 8(*d*), captures all the qualitative features present in

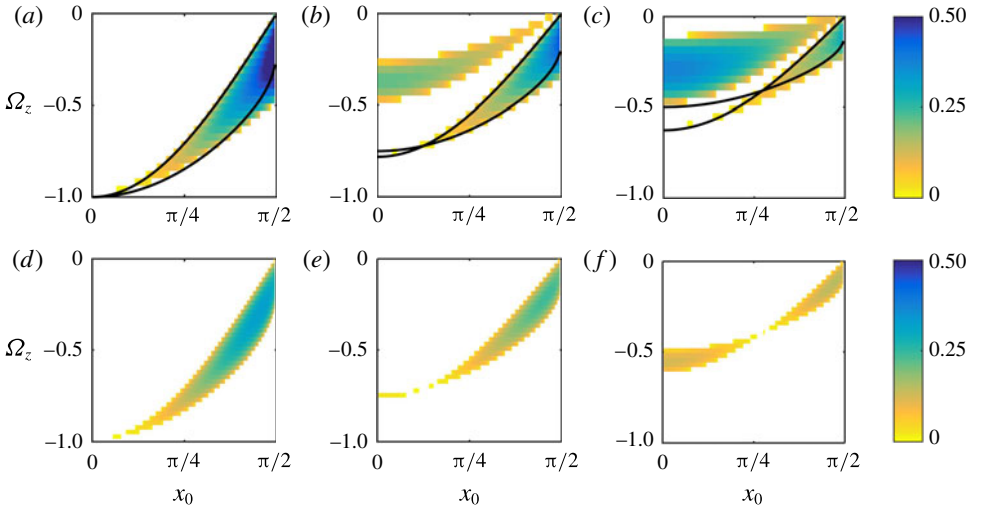

FIGURE 8. (Colour online) (*a–c*) σ_N and (*d–f*) σ_C^* plotted as a function of x_0 and Ω_z for Taylor–Green vortices with (*a,d*) $E=1$, (*b,e*) $E=0.75$ and (*c,f*) $E=0.5$. White regions in the plots correspond to $\mathrm{Re}[\sigma_N, \sigma_C^*] \leqslant 0$. All the plots correspond to $\tau=0$. The two solid black curves in each of (*a*), (*b*) and (*c*), described by (4.2) and (4.3), correspond to the boundaries of the unstable domain in (*d*), (*e*) and (*f*), respectively.

the σ_N distribution in 8(*a*) with reasonable quantitative agreement in the domain of instability and growth rates.

For $E=0.75$, which corresponds to more strongly non-axisymmetric streamlines in comparison to $E=1$, two domains of instability are seen in the σ_N distribution (figure 8*b*). The instability domain that extends from around $x_0=0$, $\Omega_z=-0.5$ is probably a non-centrifugal instability as it is continuously connected to the instability present at $\Omega_z=0$. We recall, based on the discussion in § 3.1, that the Taylor–Green vortices are centrifugally stable at $\Omega_z=0$ if there is no axial flow. The other instability domain, associated with the centrifugal instability, is similar to the unstable domain captured by σ_C^* in figure 8(*e*). For $E=0.5$, corresponding to strongly non-axisymmetric streamlines, the non-centrifugal instability domain in the σ_N distribution (figure 8*c*) is larger than that for $E=0.75$, with the corresponding centrifugal instability domain being smaller. The criterion based on σ_C^* (figure 8*f*) captures the centrifugal instability domain reasonably well, albeit with an extra feature near $x_0 \approx 0$, $\Omega_z \approx -0.5$ that is not present in the σ_N distribution.

3.4. *Axial flow and background rotation*

In this section, we consider axial flows quantified by $\tau=0.3$ and $\tau=1.0$ for both the Stuart vortices and the Taylor–Green vortices.

3.4.1. *Stuart vortices*

There exists at least one unstable streamline for almost the entire plane of $0<\rho<1$ and $-2.5<\Omega_z<0$ for Stuart vortices with $\tau=0.3$ and $\tau=1$. We therefore refrain from showing a contour plot like figure 3 as it would indicate instability almost over the entire ρ–Ω_z plane.

Colour plots of σ_N and σ_C^* on the $\tilde{\psi}$–Ω_z plane for $\rho=0.9$, 0.745 and 0.337 at $\tau=0.3$ are shown in figure 9. For all three values of ρ, there exist streamlines that

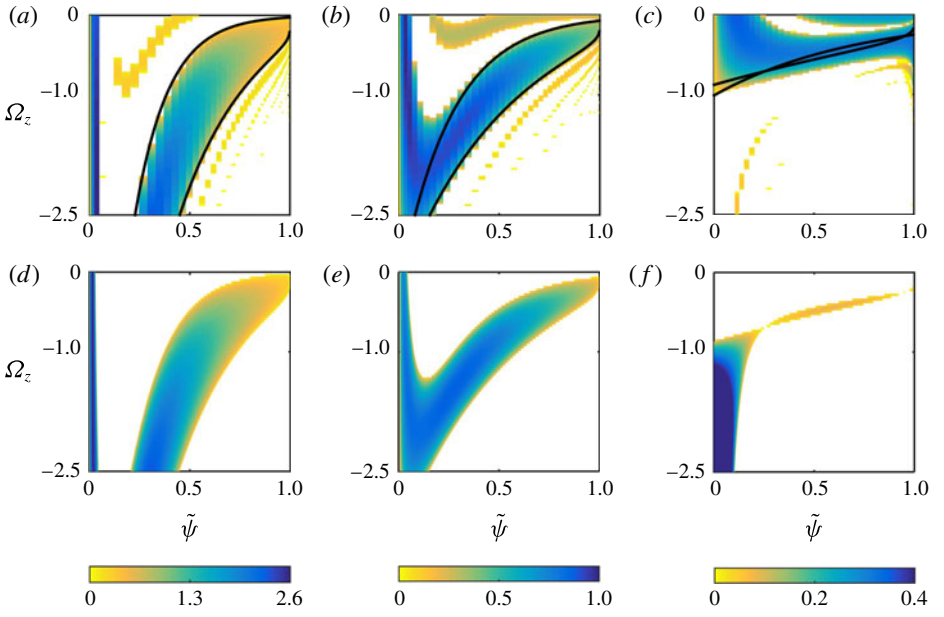

FIGURE 9. (Colour online) Colour plot of (*a–c*) σ_N and (*d–f*) σ_C^* as a function of $\tilde{\psi}$ and Ω_z for Stuart vortices with (*a*,*d*) $\rho = 0.9$, (*b*,*e*) $\rho = 0.745$ and (*c*,*f*) $\rho = 0.337$. White regions in the plots correspond to $\mathrm{Re}[\sigma_N, \sigma_C^*] \leqslant 0$. All the plots correspond to $\tau = 0.3$. The solid black curves in (*a–c*) show the $-|\Omega_z|_{L,C}$ versus $\tilde{\psi}$ and $-|\Omega_z|_{U,C}$ versus $\tilde{\psi}$ variations, as described by (4.2) and (4.3).

display a threshold of $|\Omega_z| = |\Omega_z|_{L,N}$ above which they become unstable and a higher threshold of $|\Omega_z| = |\Omega_z|_{U,N}$ above which they become stable (figure 9*a–c*). For $\rho = 0.9$ and 0.745, the streamlines in the immediate neighbourhood around the origin ($\tilde{\psi} \leqslant 0.05$) are unstable for all $\Omega_z > -2.5$; this set of unstable streamlines is absent for $\tau = 0$. The colour plots of σ_C^* are in remarkable qualitative and quantitative agreement with those of σ_N for $\rho = 0.9, 0.745$ (figure 9*d*,*e*), but compare poorly with σ_N for the strongly elliptic scenario of $\rho = 0.337$ (figure 9*f*).

For $\tau = 1$, which corresponds to a stronger axial flow than $\tau = 0.3$, the colourmaps of σ_N and σ_C^* are shown in figure 10. The results are qualitatively similar to those of $\tau = 0.3$, with the existence of two thresholds $|\Omega_z|_{L,N}$ and $|\Omega_z|_{U,N}$, between which the streamlines away from the origin are unstable for $\rho = 0.9, 0.745$ (figure 10*a*,*b*). Also, as shown in figure 10(*a*,*b*), $\tau = 1$ corresponds to a larger (compared to $\tau = 0.3$) range of streamlines around the origin that are unstable for all $\Omega_z > -2.5$. The colourmaps based on σ_C^* continue to be in good qualitative and quantitative agreement with σ_N for $\rho = 0.9, 0.745$, whereas the agreement is poor for $\rho = 0.337$.

The threshold values $|\Omega_z|_{L,N}$ and $|\Omega_z|_{U,N}$ are, in general, functions of both ρ and $\tilde{\psi}$. $|\Omega_z|_{L,N}$, the threshold above which a given streamline becomes centrifugally unstable, decreases with an increase in τ, consistent with the observations of Mathur *et al.* (2014) that an increase in τ increases the likelihood of centrifugal instability. However, the larger threshold value $|\Omega_z|_{U,N}$, above which a given streamline becomes centrifugally stable, is invariant with τ. As a consequence, for large enough $|\Omega_z|$, streamlines far from the origin remain centrifugally stable even for large values of τ, thus suggesting that the results of Mathur *et al.* (2014) for $\Omega_z = 0$ cannot be

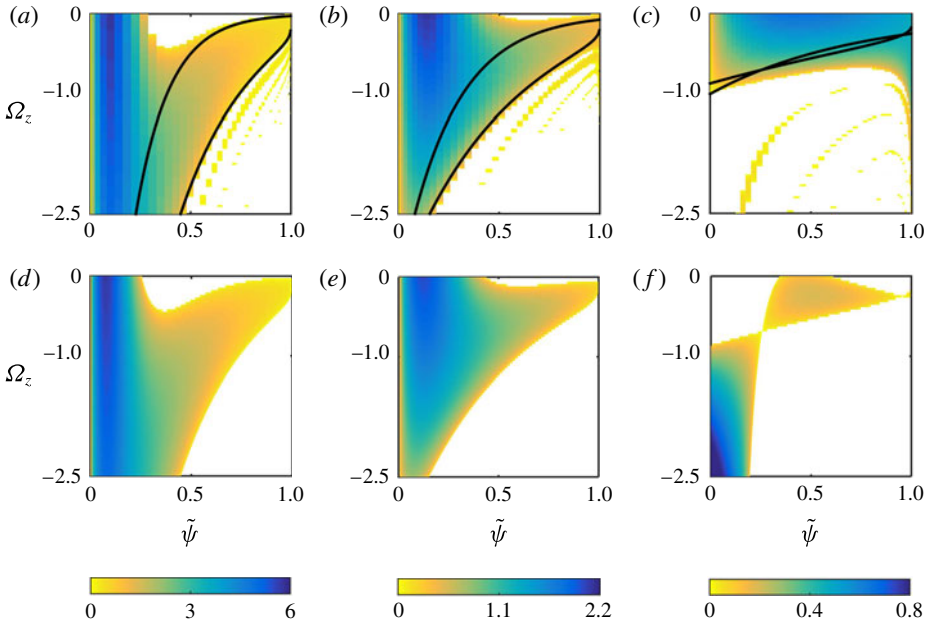

FIGURE 10. (Colour online) Colour plot of (*a–c*) σ_N and (*d–f*) $\sigma^*_{\boldsymbol{c}}$ as a function of $\tilde{\psi}$ and Ω_z for Stuart vortices with (*a*,*d*) $\rho = 0.9$, (*b*,*e*) $\rho = 0.745$ and (*c*,*f*) $\rho = 0.337$. White regions in the plots correspond to $\mathrm{Re}[\sigma_N, \sigma^*_{\boldsymbol{c}}] \leqslant 0$. All the plots correspond to $\tau = 1.0$. The solid black curves in (*a–c*) show the $-|\Omega_z|_{L,\boldsymbol{c}}$ versus $\tilde{\psi}$ and $-|\Omega_z|_{U,\boldsymbol{c}}$ versus $\tilde{\psi}$ variations, as described by (4.2) and (4.3).

extended to the case of $\Omega_z \neq 0$. Similarly, owing to a new set of streamlines around the origin becoming centrifugally unstable for $\tau > 0$, the $\tau = 0$ results cannot be simply extended to the case of $\tau > 0$. The relevance of the solid black curves in figures 9(*a–c*) and 10(*a–c*) is discussed in § 4.

3.4.2. *Taylor–Green vortices*

We consider axial velocity strengths of $\tau = 0.3$ and $\tau = 1.0$ in this subsection too. Figure 11 shows the variations of $\sigma^*_{\boldsymbol{c}}$ and σ_N as a function of x_0 and Ω_z for three different values of E at $\tau = 0.3$. For $E = 1$, as shown in figure 11(*a*,*d*), the variation in $\sigma^*_{\boldsymbol{c}}$ is in close agreement with σ_N over the entire x_0–Ω_z plane, with some differences in the growth rate magnitudes for the streamlines close to the edge of the vortex ($x_0 \lesssim \pi/2$).

For $E = 0.75$, a new smaller domain of instability emerges close to $\Omega_z = 0$ in the σ_N distribution (figure 11*b*), whereas $\sigma^*_{\boldsymbol{c}}$ does not pick up this new instability domain (figure 11*e*). While $\sigma^*_{\boldsymbol{c}}$ captures the centrifugal instability for $x_0 \gtrsim 0.51$, it does not predict the instability present in the region $x_0 \lesssim 0.51$, $\Omega_z \geqslant -0.7$ and wrongly predicts instability for $x_0 \leqslant 0.39$, $\Omega_z \leqslant -0.707$. The comparison between σ_N and $\sigma^*_{\boldsymbol{c}}$ for $E = 0.5$ is qualitatively similar to that of $E = 0.75$, albeit with a larger domain for which $\sigma^*_{\boldsymbol{c}}$ wrongly predicts instability. Upon increasing the axial velocity parameter τ to 1.0 (figure 12), we observe an improvement in the agreement between $\sigma^*_{\boldsymbol{c}}$ and σ_N. Specifically, the existence of two separate bands of unstable streamlines for a fixed Ω_z is predicted by $\sigma^*_{\boldsymbol{c}}$ for $E = 1$ and $E = 0.75$.

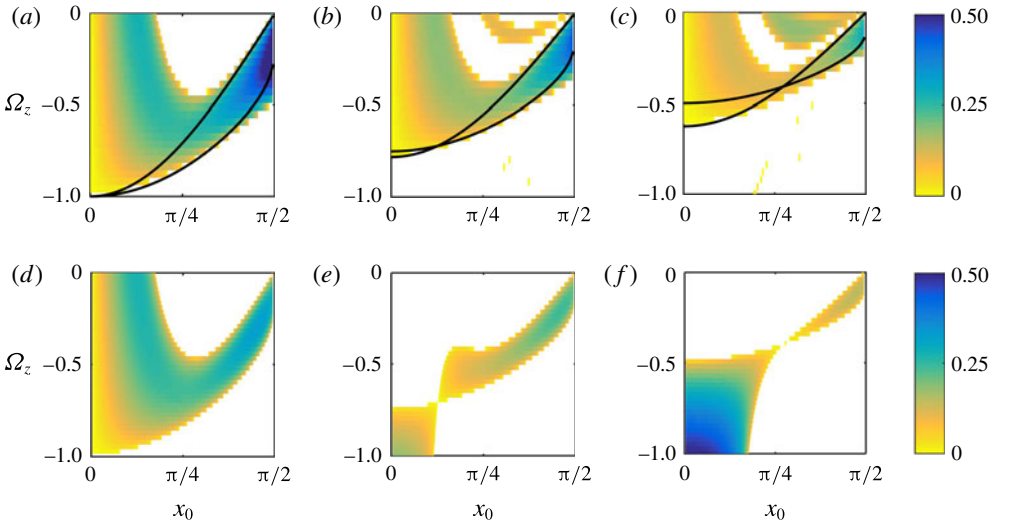

FIGURE 11. (Colour online) Colour plot of (*a–c*) σ_N and (*d–f*) $\sigma_{\boldsymbol{C}}^*$ as a function of x_0 and Ω_z for Taylor–Green vortices with (*a,d*) $E = 1$, (*b,e*) $E = 0.75$ and (*c,f*) $E = 0.5$. White regions in the plots correspond to $\mathrm{Re}[\sigma_N, \sigma_{\boldsymbol{C}}^*] \leqslant 0$. All the plots correspond to $\tau = 0.3$. The solid black curves in (*a–c*) show the $-|\Omega_z|_{L,\boldsymbol{C}}$ versus x_0 and $-|\Omega_z|_{U,\boldsymbol{C}}$ versus x_0 variations, as described by (4.2) and (4.3).

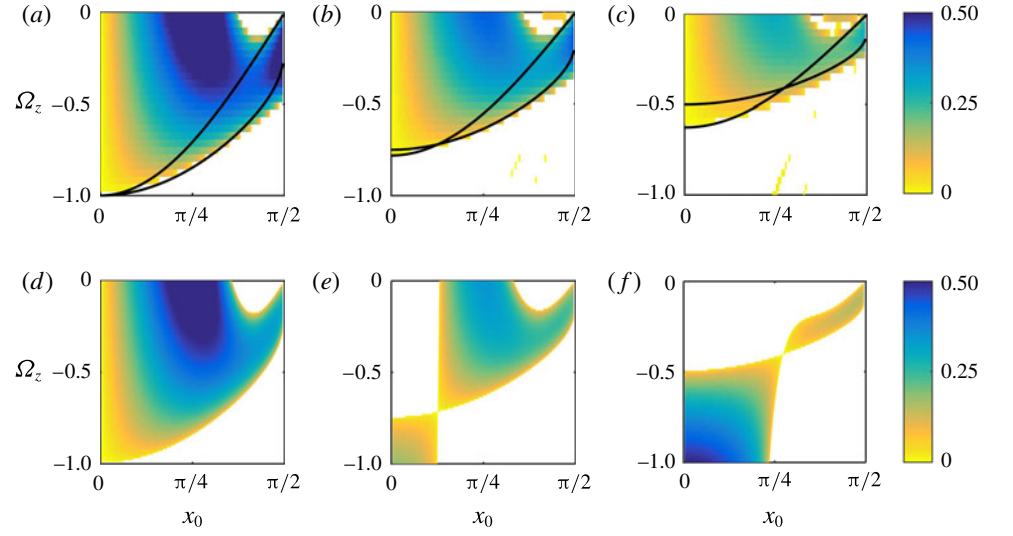

FIGURE 12. (Colour online) Colour plot of (*a–c*) σ_N and (*d–f*) $\sigma_{\boldsymbol{C}}^*$ as a function of x_0 and Ω_z for Taylor–Green vortices with (*a,d*) $E = 1$, (*b,e*) $E = 0.75$ and (*c,f*) $E = 0.5$. White regions in the plots correspond to $\mathrm{Re}[\sigma_N, \sigma_{\boldsymbol{C}}^*] \leqslant 0$. All the plots correspond to $\tau = 1.0$. The solid black curves in (*a–c*) show the $-|\Omega_z|_{L,\boldsymbol{C}}$ versus x_0 and $-|\Omega_z|_{U,\boldsymbol{C}}$ versus x_0 variations, as described by (4.2) and (4.3).

Similar to the thresholds introduced in the discussion of figure 8 for $\tau = 0$, we define corresponding $|\Omega_z|_{L,N}$ and $|\Omega_z|_{U,N}$ for the centrifugal instability domains for each x_0 in figures 11(*a–c*) and 12(*a–c*). The lower threshold $|\Omega_z|_{L,N}$ for streamlines with $x_0 \leqslant 0.55$ is zero for $\tau = 0.3$ and $E = 1$ (figure 11*a*). The corresponding range of

streamlines for which $|\Omega_z|_{L,N} = 0$ at $\tau = 0.3$ are $x_0 \leqslant 0.5$ and $x_0 \leqslant 0.46$ for $E = 0.75$ and $E = 0.5$, respectively. With a further increase in τ to 1, the range of streamlines with $|\Omega_z|_{L,N} = 0$ spreads to larger values of x_0. For a small range of streamlines close to the edge of the vortex, $|\Omega_z|_{L,N}$ is invariant with τ for $\tau \leqslant 1$.

For each of $E = 1$, 0.75 and 0.5, the variation of $|\Omega_z|_{U,N}$ as a function of x_0 is independent of τ. Recalling that the threshold $|\Omega_z|_{2,N}$ corresponds to $Ro = 1$ for all E in figure 6, we conclude that the criterion $Ro < 1$ for centrifugal stability in anticyclonic Taylor–Green vortices is independent of E and τ for $\tau \leqslant 1$. The significance of the solid black curves in figures 11(*a–c*) and 12(*a–c*), which capture the upper threshold $|\Omega_z|_{U,N}$ well, is discussed in § 4.

4. Discussion and conclusions

In this paper, we derived a criterion for centrifugal instability in an axisymmetric vortex with axial flow and background rotation. The criterion was then heuristically extended to non-axisymmetric vortices. The resulting non-axisymmetric criterion (2.10), which converges to the criterion of Bayly (1988) in the absence of background rotation and axial flow, was then evaluated for two different vortex models: the Stuart vortices and the Taylor–Green vortices. For Taylor–Green vortices with no background rotation and large axial flow, $\sigma^*_{\boldsymbol{C}}$ is shown to be reasonably accurate for streamlines satisfying $S \lesssim 0.2$, with S being the extent of non-axisymmetry. An investigation of how the threshold axial flow, beyond which centrifugal instability emerges in Taylor–Green vortices with no background rotation, varies as a function of x_0 and E would be worthwhile.

For Stuart and Taylor–Green vortices without an axial flow, the criterion (2.10) based on $\sigma^*_{\boldsymbol{C}}$ performs remarkably well in delineating the stable and unstable regions in the ρ–Ω_z and E–Ω_z planes, respectively. This criterion is also shown to perform qualitatively and quantitatively better than the sufficient criterion proposed by Sipp & Jacquin (2000). In the presence of both axial flow and background rotation, our criterion accurately predicts the range of centrifugally unstable streamlines and their growth rates for sufficiently large values of ρ and E.

We now explain some of the numerical results in § 3 using the criterion in (2.10). In the absence of an axial flow, the criterion for instability in (2.10) reduces to

$$-(\sigma^*_{\boldsymbol{C}\{1,2\}})^2 = \left(\frac{4\pi}{T} + 2\Omega_z\right)\left(\frac{1}{T}\frac{\mathrm{d}\Gamma}{\mathrm{d}\psi} + 2\Omega_z\right) < 0, \tag{4.1}$$

as already shown in (3.5). Restricting our analysis to streamlines in vortices for which T and $\mathrm{d}\Gamma/\mathrm{d}\psi$ are both positive, we consider the variation of $(\sigma^*_{\boldsymbol{C}\{1,2\}})^2$ with Ω_z. At $\Omega_z = 0$, the criterion in (4.1) is not satisfied, and the corresponding streamline is centrifugally stable. As Ω_z is decreased from zero, $(\sigma^*_{\boldsymbol{C}\{1,2\}})^2$ becomes positive first at $\Omega_z = (-1/2T)\min(4\pi, \mathrm{d}\Gamma/\mathrm{d}\psi)$. For every streamline in figures 5(*b*,*e*) and 8(*d–f*), the threshold $|\Omega_z|_{L,\boldsymbol{C}}$ is therefore given by

$$|\Omega_z|_{L,\boldsymbol{C}} = (1/2T)\min(4\pi, \mathrm{d}\Gamma/\mathrm{d}\psi), \tag{4.2}$$

with the $\boldsymbol{C}$ in the subscript referring to the criterion in (4.1). The above threshold is an estimate of the threshold $|\Omega_z|_{L,N}$ found in the corresponding σ_N distributions. The outermost streamline in both Stuart ($x_0 = \pi$) and Taylor–Green ($x_0 = \pi/2$) vortices corresponds to $T \to \infty$, thus resulting in $|\Omega_z|_{L,\boldsymbol{C}} = 0$ based on (4.2).

Upon increasing $|\Omega_z|$ further beyond $|\Omega_z|_{L,\boldsymbol{C}}$ for a given streamline, $(\sigma^*_{\boldsymbol{C}\{1,2\}})^2$ becomes negative again at

$$|\Omega_z|_{U,\boldsymbol{C}} = (1/2T)\max(4\pi, \mathrm{d}\Gamma/\mathrm{d}\psi), \tag{4.3}$$

which is an estimate of the threshold $|\Omega_z|_{U,N}$ above which the streamline becomes centrifugally stable based on σ_N.

In Stuart vortices with no axial flow ($\tau = 0$), $|\Omega_z|_{L,\boldsymbol{C}}$ and $|\Omega_z|_{U,\boldsymbol{C}}$ accurately capture the centrifugally unstable domain on the $\tilde{\psi}$–Ω_z plane for both $\rho = 0.745$ (solid black curves in figure 5*a*) and $\rho = 0.602$ (solid black curves in figure 5*d*). We recall that the maximum of $|\Omega_z|_{U,\boldsymbol{C}}$ among all the streamlines for a given ρ represents the threshold $|\Omega_z|_{2,\boldsymbol{C}}$ plotted in figure 3.

In the presence of an axial flow, the upper threshold estimate $|\Omega_z|_{U,\boldsymbol{C}}$ in (4.3) remains remarkably accurate in predicting the maximum magnitude of rotation above which streamlines in the Stuart vortices with $\rho = 0.9$ and $\rho = 0.745$ become centrifugally stable (the bottom solid black curves in figures 9*a*,*b* and 10*a*,*b*). The lower threshold $|\Omega_z|_{L,\boldsymbol{C}}$, however, does not capture the centrifugal instability induced by the axial flow effects in the streamlines around the origin.

In Taylor–Green vortices, $|\Omega_z|_{L,\boldsymbol{C}}$ is accurate in describing the lower threshold for $\tau = 0$ (figure 8*a*–*c*) whereas $|\Omega_z|_{U,\boldsymbol{C}}$ remains accurate even in the presence of axial flow (figures 8*a*–*c*, 11*a*–*c* and 12*a*–*c*). In summary, $|\Omega_z|_{U,\boldsymbol{C}}$ represents a reasonably accurate estimate of $|\Omega_z|_{U,N}$ for both Stuart and Taylor–Green vortices with $\tau \leqslant 1$, and hence its maximum among all streamlines represents an estimate of $|\Omega_z|_{2,N}$ beyond which the vortex with a specific value of ρ or E is centrifugally stable.

An interesting observation based on figures 9(*f*), 10(*f*), 11(*e*,*f*) and 12(*e*,*f*) is that $\sigma^*_{\boldsymbol{C}}$ fails to predict the instability for $|\Omega_z| < |\Omega_z|_{L,\boldsymbol{C}}$, and wrongly predicts instability well above $|\Omega_z| = |\Omega_z|_{L,\boldsymbol{C}}$ for a range of streamlines around the origin. This range of streamlines, for which $\sigma^*_{\boldsymbol{C}}$ fails, coincides with the region to the left of the point of intersection between the $|\Omega_z|_{L,\boldsymbol{C}}$ and $|\Omega_z|_{U,\boldsymbol{C}}$ curves plotted in the corresponding σ_N figures. The point of intersection between $|\Omega_z|_{L,\boldsymbol{C}}$ and $|\Omega_z|_{U,\boldsymbol{C}}$ occurs at $\mathrm{d}\Gamma/\mathrm{d}\psi = 4\pi$, and the criterion based on $\sigma^*_{\boldsymbol{C}}$ (2.10) is therefore observed to fail on streamlines with $\mathrm{d}\Gamma/\mathrm{d}\psi > 4\pi$ in the presence of background rotation and/or axial flow.

In the case of cyclonic rotation, i.e. $\Omega_z > 0$, the criterion in (4.1) is not satisfied for all Ω_z if $T > 0$ and $\mathrm{d}\Gamma/\mathrm{d}\psi > 0$. Therefore, a centrifugally stable vortex (with no axial flow and background rotation) remains centrifugally stable with the addition of cyclonic rotation, a result consistent with the results of Sipp *et al.* (1999). It would furthermore be worthwhile to investigate the validity of (2.10) in describing centrifugal instability in vortices that are centrifugally unstable even without axial flow and background rotation.

The heuristic transformation from the axisymmetric to non-axisymmetric criterion presented in § 2 is not unique, and other ways of expressing criterion (2.8) in terms of Γ and T could be explored. For example, the denominator of the first term in criterion (2.8) could also be rewritten to give

$$(\sigma^*_{\boldsymbol{C}\{1,2\}})^2 = \left[\frac{4(\mathrm{d}w/\mathrm{d}\psi)^2(\Omega_z + \psi'/r)^2}{(1/r^2)(\mathrm{d}(r\psi')/\mathrm{d}\psi - 2)^2 + (\mathrm{d}w/\mathrm{d}\psi)^2} - 2\left(\frac{\psi'}{r} + \Omega_z\right)\left(\frac{\psi'}{r}\frac{\mathrm{d}(r\psi')}{\mathrm{d}\psi} + 2\Omega_z\right)\right] > 0, \tag{4.4}$$

which would then not involve $\mathrm{d}T/\mathrm{d}\psi$ when ψ' and r are written in terms of Γ and T. It would be interesting to evaluate the accuracy of the resulting criterion, which would

still converge to the exact criterion of Bayly (1988) for $\Omega_z = 0$ and $\tau = 0$, in describing centrifugal instability in non-axisymmetric vortices. An exact analytical criterion to describe centrifugal instability in arbitrarily non-axisymmetric vortices remains elusive.

Acknowledgements

We thank J.-M. Chomaz for suggesting the form of figure 3. We also thank the anonymous referees for their comments which helped improve the paper.

REFERENCES

BAYLY, B. J. 1988 Three-dimensional centrifugal-type instabilities in inviscid two-dimensional flows. *Phys. Fluids* **31**, 56–64.

BILLANT, P. & GALLAIRE, F. 2005 Generalized Rayleigh criterion for non-axisymmetric centrifugal instabilities. *J. Fluid Mech.* **542**, 365–379.

BILLANT, P. & GALLAIRE, F. 2013 A unified criterion for the centrifugal instabilities of vortices and swirling jets. *J. Fluid Mech.* **734**, 5–35.

ECKHOFF, K. S. 1984 A note on the instability of columnar vortices. *J. Fluid Mech.* **145**, 417–421.

GALLAIRE, F. & CHOMAZ, J. M. 2003*a* Instability mechanisms in swirling flows. *Phys. Fluids* **15**, 2622–2639.

GALLAIRE, F. & CHOMAZ, J. M. 2003*b* Mode selection in swirling jet experiments: a linear stability analysis. *J. Fluid Mech.* **494**, 223–253.

GODEFERD, F. S., CAMBON, C. & LEBLANC, S. 2001 Zonal approach to centrifugal, elliptic and hyperbolic instabilities in Stuart vortices with external rotation. *J. Fluid Mech.* **449**, 1–37.

HOPFINGER, E. J. & VAN HEIJST, G. J. F. 1993 Vortices in rotating fluids. *Annu. Rev. Fluid Mech.* **25**, 241–289.

KLOOSTERZIEL, R. C. & VAN HEIJST, G. J. F. 1991 An experimental study of unstable barotropic vortices in a rotating fluid. *J. Fluid Mech.* **223**, 1–24.

LEBLANC, S. & CAMBON, C 1998 Effects of the Coriolis force on the stability of Stuart vortices. *J. Fluid Mech.* **356**, 353–379.

LEIBOVICH, S. & STEWARTSON, K. 1983 A sufficient condition for the instability of columnar vortices. *J. Fluid Mech.* **126**, 335–356.

LIFSCHITZ, A. & HAMEIRI, E. 1991 Local stability conditions in fluid dynamics. *Phys. Fluids* A **3**, 2644–2651.

MATHUR, M., ORTIZ, S., DUBOS, T. & CHOMAZ, J. M. 2014 Effects of an axial flow on the centrifugal, elliptic and hyperbolic instabilities in Stuart vortices. *J. Fluid Mech.* **758**, 565–585.

MUTABAZI, I., NORMAND, C. & WESFREID, J. E. 1992 Gap size effects on centrifugally and rotationally driven instabilities. *Phys. Fluids* A **4**, 1199–1205.

POTYLITSIN, P. G. & PELTIER, W. R. 1999 Three-dimensional destabilization of Stuart vortices: the influence of rotation and ellipticity. *J. Fluid Mech.* **387**, 205–226.

POTYLITSIN, P. G. & PELTIER, W. R. 2003 On the nonlinear evolution of columnar vortices in a rotating environment. *Geophys. Astrophys. Fluid Dyn.* **97**, 365–391.

RAYLEIGH, LORD 1917 On the dynamics of revolving fluids. *Proc. R. Soc. Lond.* A **93**, 148–154.

SIPP, D. & JACQUIN, L. 1998 Elliptic instability in two-dimensional flattened Taylor–Green vortices. *Phys. Fluids* **10**, 839–849.

SIPP, D. & JACQUIN, L. 2000 Three-dimensional centrifugal-type instabilities of two-dimensional flows in rotating systems. *Phys. Fluids* **12**, 1740–1748.

SIPP, D., LAUGA, E. & JACQUIN, L. 1999 Vortices in rotating systems: centrifugal, elliptic and hyperbolic type instabilities. *Phys. Fluids* **11**, 3716–3728.

STUART, J. T. 1967 On finite amplitude oscillations in laminar mixing layers. *J. Fluid Mech.* **29**, 417–440.

TAYLOR, G. I. & GREEN, A. E. 1937 Mechanism of the production of small eddies from large ones. *Proc. R. Soc. Lond.* A **158**, 499–521.